Electronic Supplementary Material (ESI) for Physical Chemistry Chemical Physics.

Supplementary Information

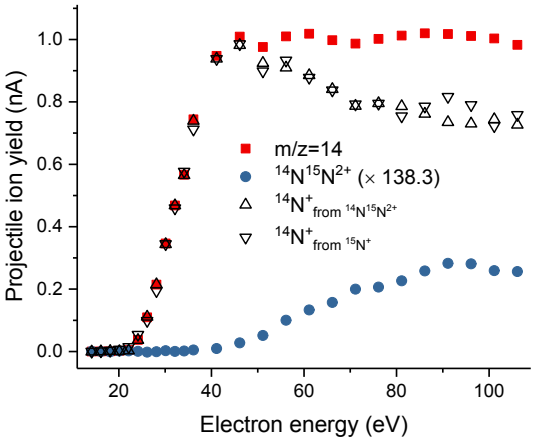

Fig. S1 Contribution of $^{14}N^+$ and $^{14}N_2^{2+}$ to the projectile ion yield at m/z=14 as a function of the electron energy upon electron ionization of N_2.

As the appearance energy for N^+ upon electron ionization of N_2 is with 24.3 eV[42] lower than the appearance energy for the isobaric doubly-charged molecular ion N_2^{2+} (42.9 eV[43]), we measured the ion yield for $^{14}N^{15}N^{2+}$ at m/z=14.5 and of the ion yield at m/z=14, which is a combination of $^{14}N^+$, $^{14}N_2^{2+}$ and $^{12}CH_2^+$. The exact mass of the hydrocarbon ion is 14.01565 Da, whereas the two nitrogen ions are located at m/z=14.003074. With a mass resolution of m/Δm of about 1100, these ions can be well separated. From the isotopic ratio of nitrogen, we deduce the contribution of $^{14}N_2^{2+}$ using the yield of $^{14}N^{15}N^{2+}$. In Fig. S1 the blue solid circles represent the yield of $^{14}N^{15}N^{2+}$ multiplied with the reciprocal value of the relative abundance of this isotopologue. The rest of the ion signal at m/z=14 is assigned to the singly-charged fragment ion $^{14}N^+$ (open triangles). As an additional check, we look, if the yield of $^{15}N^+$ agrees according to the isotopic abundance with the ion yield determined for $^{14}N^+$ (open diamonds). As a compromise between ion yield and suppression of the dication, we operated the ion source at 50 eV. This explains the small contribution of N_2^{2+} in our N^+ measurements.

Fig. S2 and Fig. S3 show enlarged sections of mass spectra at m/z=32 and m/z=44. The solid line represents the product ion spectrum of a fresh propanethiol SAM upon Ar^+ irradiation and the red dashed line corresponds to product ion mass spectra obtained after several hours of Ar^+ irradiation, where the SAM film was removed by sputtering. The thin vertical lines represent exact masses for product ions that can be expected to be formed. In both figures, a low-mass isobaric ion can be assigned to a sulfur containing species, i.e., S^+ at m/z=32 and CS^+ at m/z=44.

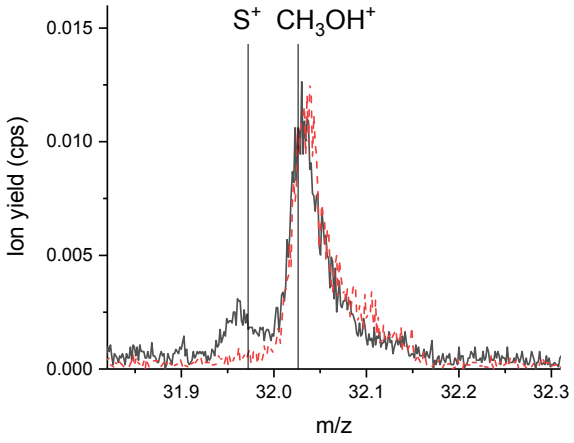

Fig. S2 Section of mass spectra obtained during 69 eV Ar^+ bombardment at a current of 1.4 nA of a propanethiol SAM. The black solid line was obtained for a fresh SAM target and the red dashed line was obtained after several hours of Ar^+ irradiation. The peak slightly below m/z=32 can be assigned to S^+ with the exact mass indicated by a thin vertical line. The peak slightly above m/z=32 fits nicely to a methanol cation which originates from the residual gas, most likely from the cleaning procedure of the instrument.

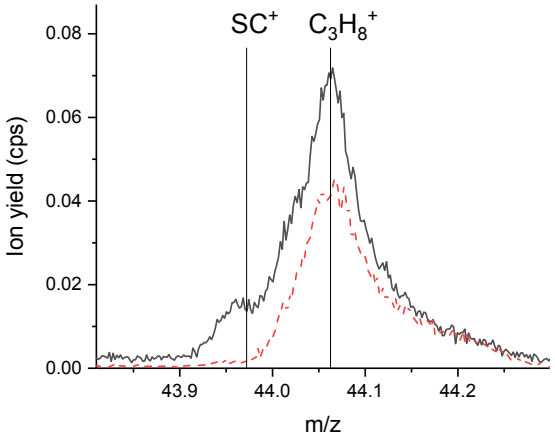

Fig. S3 Section of mass spectra obtained during 69 eV Ar^+ bombardment at a current of 1.4 nA of a propanethiol SAM. The black solid line was obtained for a fresh SAM target and the red dashed line was obtained after several hours of Ar^+ irradiation. The peak slightly below m/z=44 can be assigned to SC^+ with the exact mass indicated by a thin vertical line. The peak slightly above m/z=44 fits nicely to a propane cation. After removal of the SAM, only the $C_3H_8^+$ remains, which originates from the residual gas, most likely from cracked pump oil residuum, usually assumed to consist mostly of C7 and C8 hydrocarbons.

In Fig. S4 the effect of sputter-cleaning of a target surface upon ion irradiation is demonstrated. Although the vacuum in the surface chamber is below 10^{-6} Pa, residual gas consisting predominantly of H_2O, air from tiny leaks and hydrocarbons from solvents and cracked pumping oils, quickly adsorb to clean surfaces (1 ML in about 100 s at this pressure). The impinging projectile ions remove some of these adsorbed molecules as sputtered neutrals as well as product ions

that can be seen by SurfTOF. For every projectile ion current as well as projectile species and collision energy, a different steady-state condition between newly attaching molecules and the removal by the projectile ions will form. By lowering the projectile ion current from 14 nA to 1 nA, the removal of adsorbate molecules is reduced and it takes a few minutes until a new steady-state film is formed. It is interesting to note, that in Fig. S4 the steady-state yield for m/z=27 dropped from 5.4 cps to 3.5 cps (to ~ 65%) whereas the value for m/z=29 dropped from 3.2 cps to 1.5 cps (to ~ 47%). This also demonstrates the advantage of a clean and well-defined SAM surface compared to a hydrocarbon adsorbate layer as used earlier[20].

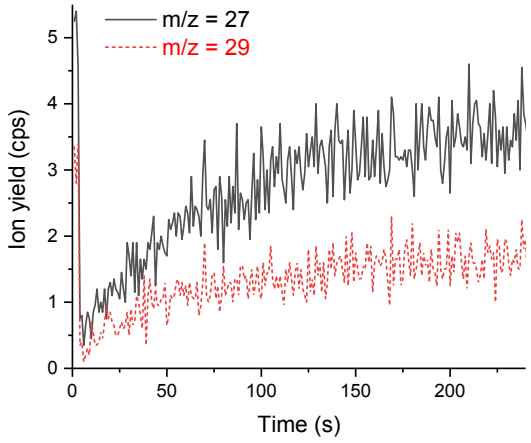

Fig. S4 Effect of the adsorption of hydrocarbon molecules from cracked pumping oil a gold surface. The ion yields of $C_2H_3^+$ at m/z=27 and $C_2H_5^+$ at m/z=29 are measured as a function of the irradiation time with Ar^+ at 70 eV collision energy. Bombarding the surface with a high projectile ion current of 14 nA removes efficiently the adsorbate layer by sputter-cleaning and the formation pf product ions formed upon fragmentation and ionization of hydrocarbon molecules originating from cracked pumping oils. When lowering the projectile current to 1 nA, the yields of these product ions drop rapidly and reach an equilibrium value after a few minutes, during which a new steady-state adsorbate layer is formed.

Calculations of bond dissociation energies of various bonds in $CH_3CH_2CH_2S$-Au_9

Methods

Calculations on clusters models were performed using the B3LYP density functional theory (DFT) functional. For H, C and S, the cc-pVDZ basis set was used; for Au, the ECP60MDF/cc-pVDZ-PP Stuttgart basis set was employed[S1,S2]. The gold cluster Au_9 was taken from Ref.[S3]. For systems that include gold atoms, two lowest spin multiplicities were tried and wavefunction stabilization was performed for each structure. Bond dissociation energies were calculated as the energy difference between optimized product structures and the optimized initial cluster, with zero-point energy included; all structures represent local minima on the potential energy surface. Calculations were performed in the Gaussian 16 software package[S4].

Results

Fig. S5 shows bond dissociation energies in $CH_3CH_3CH_2SH$ and the respective cation, showing that the C–S bond is the weakest one, followed by the central C–C bond; the terminal C–C bond is the strongest one.

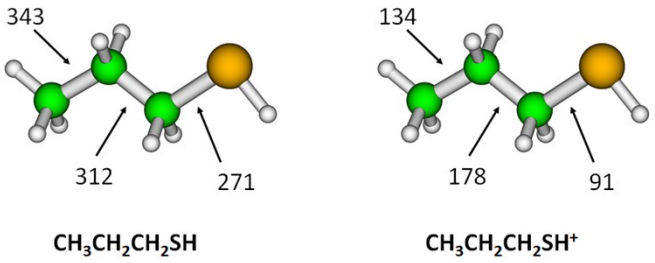

Fig. S5 Bond dissociation energies (in kJ/mol) for various bonds in $CH_3CH_2CH_2SH$ and its cation. Calculated at the B3LYP/cc-pVDZ level. The lower energy for CH_3–$CH_2CH_2SH^+$ bond dissociation (134 kJ/mol) is caused by ring formation within the CH_2CH_2SH radical after CH_3 dissociation.

Bond dissociation energies of the $CH_3CH_2CH_2S$ radical adsorbed on the Au surface was approached by modeling adsorption of the radical on $Au_9^{0/+}$. Fig. S6 shows that for the $CH_3CH_2CH_2S$ Au_9 system, the first bond to break would be S–C, followed by desorption of the whole $CH_3CH_2CH_2S$ radical and C–C bonds. For the cationic system, the relative dissociation energy of various bonds is more evenly distributed. This can explain, along with the steric hinderance due the presence of other molecules on the surface, the increased probability of C–C bond dissociation observed in the experiment.

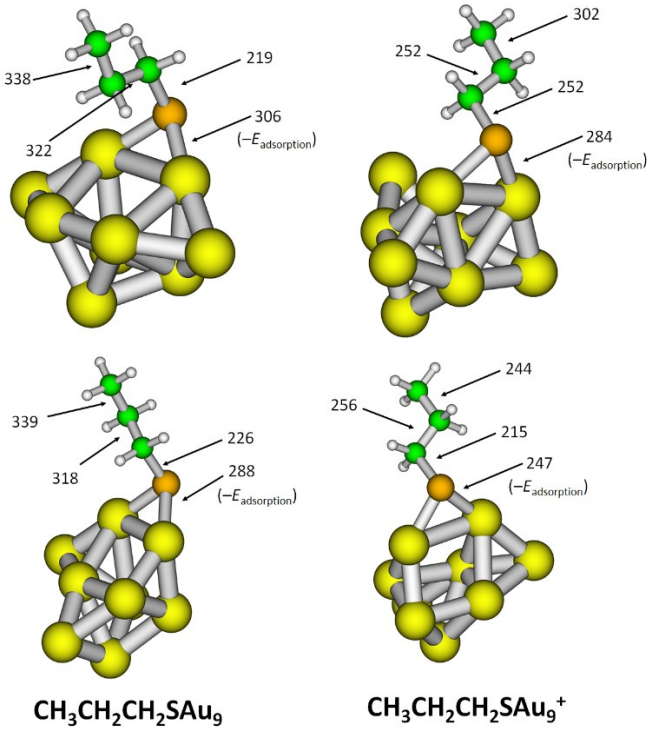

Figure S6 – Bond dissociation energies (in kJ/mol) for various bonds in $CH_3CH_2CH_2S.Au_9^{0/+}$ with two different models for each stoichiometry. Calculated at the B3LYP/cc-pVDZ(H,C,S),ECP60MDF/cc-pVDZ-PP(Au) level. For the Au–S bond, desorption of the whole $CH_3CH_2CH_2S$ radical from the cluster was considered. The lower energy for CH_3–CH_2CH_2S Au_9^+ bond dissociation is caused by ring formation within the CH_2CH_2S moiety after CH_3 dissociation.

Relevance of the present results to planetary atmospheres

The atmosphere of Titan is predominantly made of molecular nitrogen with a few percent of methane and a few tenths of a percent of molecular hydrogen. The ion density in Titans ionosphere measured by the Ion and Neutral Mass Spectrometer (INMS) onboard the Cassini spacecraft is dominated by N_2^+ (324.5 ions/cm^3) compared to an ion signal of 5.2 ions/cm^3 at m/z=27 (predominantly HCN^+) and 0.9 ions/cm^3 at m/z=14 (N^+)[S5]. The orbiting velocity of Titan is 5.6km/s and from Saturn 9.7 km/s. These velocities result in a collision energy in the center of mass frame of a carbonaceous meteorite particle with N_2^+ below 20 eV. This is much lower than the collision energy required for N_2^+ to trigger HCN^+ formation in our experiment of about 60 eV. The low activation energy for N^+ enables a reaction with carbon particles entering the ionosphere of Titan, however, the low density of N^+ makes this process also unlikely. The fluence of ions in Titans ionosphere can be calculated from the ion density and the velocity of a dust particle. We again take the speed of Saturn and obtain a value of about 3.3×10^6 ions per second and per mm^2. In our experiment the fluence of ions was set to 1.2×10^{10}, which is about 4000 times larger. The fluence of N^+ in Titans ionosphere is even another factor 400 lower.

Existing models of Titans ionosphere that are based on gas phase reactions reproduce nicely the measured ion densities for HCN^+ and other low-mass ions[S6]. It seems that for Titan, a pathway via ion surface reactions is not very important, most likely due to the low velocity of this moon. However, for Earth or exoplanets orbiting closer to their primary bodies the collision energy of N_2^+ and meteoritic particles easily exceeds 60 eV where reactions between N_2^+ and carbon containing surfaces are possible.

References

S1. D. Figgen, G. Rauhut, M. Dolg and H. Stoll, *Chem. Phys.*, 2005, **311**, 227-244. DOI: 10.1016/j.chemphys.2004.10.005

S2. K. A. Peterson and C. Puzzarini, *Theor. Chem. Acc.* 2005, **114**, 283-296. DOI: 10.1007/s00214-005-0681-9

S3. J. P. K. Doye and D. J. Wales, *New J. Chem.* 1998, **22**, 733-744. DOI: 10.1039/a709249k

S4. Gaussian 16, Revision C.01, M. J. Frisch, G. W. Trucks, H. B. Schlegel, G. E. Scuseria, M. A. Robb, J. R. Cheeseman, G. Scalmani, V. Barone, G. A. Petersson, H. Nakatsuji, X. Li, M. Caricato, A. V. Marenich, J. Bloino, B. G. Janesko, R. Gomperts, B. Mennucci, H. P. Hratchian, J. V. Ortiz, A. F. Izmaylov, J. L. Sonnenberg, D. Williams-Young, F. Ding, F. Lipparini, F. Egidi, J. Goings, B. Peng, A. Petrone, T. Henderson, D. Ranasinghe, V. G. Zakrzewski, J. Gao, N. Rega, G. Zheng, W. Liang, M. Hada, M. Ehara, K. Toyota, R. Fukuda, J. Hasegawa, M. Ishida, T. Nakajima, Y. Honda, O. Kitao, H. Nakai, T. Vreven, K. Throssell, J. A. Montgomery, Jr., J. E. Peralta, F. Ogliaro, M. J. Bearpark, J. J. Heyd, E. N. Brothers, K. N. Kudin, V. N. Staroverov, T. A. Keith, R. Kobayashi, J. Normand, K. Raghavachari, A. P. Rendell, J. C. Burant, S. S. Iyengar, J. Tomasi, M. Cossi, J. M. Millam, M. Klene, C. Adamo, R. Cammi, J. W. Ochterski, R. L. Martin, K. Morokuma, O. Farkas, J. B. Foresman, and D. J. Fox, Gaussian, Inc., Wallingford CT, 2016.

S5. V. Vuitton, R. V. Yelle and M. J. McEwan, *Icarus* 2007, **191**, 722-742. DOI: 10.1016/j.icarus.2007.06.023

S6. V. Vuitton, R. V. Yelle, S. J. Klippenstein, S. M.Hörst and P.Lavvas, *Icarus* 2019, **324**, 120-197. DOI: 10.1016/j.icarus.2018.06.013